npj | computational materials

Article

Published in partnership with the Shanghai Institute of Ceramics of the Chinese Academy of Sciences

https://doi.org/10.1038/s41524-024-01364-w

Enhancing the thermal conductivity of semiconductor thin films via phonon funneling

C. Jaymes Dionne[1], Sandip Thakur[1], Nick Scholz[1], Patrick Hopkins[2,3,4] & Ashutosh Giri[1]

The second law of thermodynamics asserts that energy diffuses from hot to cold. The resulting temperature gradients drive the efficiencies and failures in a plethora of technologies. However, as the dimensionalities of materials shrink to the nanoscale regime, proper heat dissipation strategies become more challenging since the mean free paths of phonons become larger than the characteristic length scales. This leads to temperature gradients that are dependent on interfaces and boundaries, which ultimately can lead to severe thermal bottlenecks. Herein, we uncover a phenomenon which we refer to as 'phonon funneling', that allows the control of phonon transport to preferentially direct phonon energy away from geometrically confined interfacial thermal bottlenecks and into localized colder regions. This phenomenon supersedes heat diffusion based on the macroscale temperature gradients, thus introducing a nanoscale regime in which boundary scattering increases the phonon thermal conductivity of thin films, an opposite effect than what is traditionally realized. This work advances the fundamental understanding of phonon transport at the nanoscale and the role of efficient scattering methods for enhancing thermal transport.

The comprehensive understanding and control of nanoscale thermal transport processes underpins the advancements in a plethora of technologies[1–7]. For example, the high operating temperatures of modern electronics, which are fundamentally driven by the dynamics and scattering mechanisms of microscopic heat carriers, often sets the limit for their achievable efficiencies and faster working speeds[7]. This is exacerbated by the advancements in fabrication of nanoscale devices with feature sizes that can even go below 10 nm, thus leading to local hot-spots arising from severe size-effects in thermal transport where dominant heat carriers with mean free paths longer than the characteristic length scales of the devices are scattered at the boundaries[8,9]. Although modern fabrication tools have achieved such increased precisions and efficiencies to gain atomic-level control over the growth of different types of materials, a corresponding advancement in our understanding and control of the heat carrier dynamics at the nanoscale is considerably lagging. This is mainly because of the complexity of fully controlling the dynamics of the broadband energy carriers that conduct heat in different directions, thus critically limiting our ability to unravel the full potential of nanoscale devices for practical applications and efficiently overcoming their limitations imposed by severe size-effects in their thermal transport.

In dielectrics and semiconductors routinely used in microelectronic devices, spectrally broadband phonons with a wide range of mean free paths (such as that in silicon, which can span a range from a few nanometers up to several microns even at room temperature) can carry heat[10,11]. Typically, when a heat source is introduced, Fourier's law of diffusive scattering of these heat carriers establishes a smooth thermal gradient. When the dimension of the heat source is smaller than or on the order of the mean free paths of phonons, however, these heat carriers can travel ballistically with non-local heat deposition[12,13]. This leads to the breakdown of the Fourier's law near and at nanoscale hotspots and gives rise to non-Fourier heat conduction typically leading to an underestimation of the heat flow efficacy as compared to the Fourier theory predictions, which has been well-established in the past three decades[5,8,9,11,14–17].

In this regard, our understanding of the thermal transport mechanisms driven by nanoscale heat sources has mostly been shaped through theoretical works focused on solving the Boltzmann transport equation (BTE) under the relaxation time approximation with several notable conclusions on non-Fourier heat conduction[18–24]. These include (but are not limited to) the demonstration of the applicability of multi-temperature models for different phonon branches during non-equilibrium conditions[23,25] and the description of non-local transport through the Levy super-diffusion model[22,26,27]. Although these theoretical studies have shed light on the microscopic dynamics of energy carriers at localized hotspots, these models

[1]Department of Mechanical, Industrial, and Systems Engineering, University of Rhode Island, Kingston, 02881 RI, USA. [2]Department of Mechanical and Aerospace Engineering, University of Virginia, Charlottesville, 22904 VA, USA. [3]Department of Materials Science and Engineering, University of Virginia, Charlottesville, 22904 VA, USA. [4]Department of Physics, University of Virginia, Charlottesville, 22904 VA, USA. e-mail: ashgiri@uri.edu

based on the BTE are prohibitive when it comes to complex geometries and device-relevant length scales.

In practical devices, hotspots typically arise due to optical or electrical excitation where the sources have physical dimensions that are comparable to the mean free paths of energy carriers[28–31]. As such, these have been identified in pump-probe optical measurements[15,17,32–34], optoelectronics[7,8,28,29], and even in nanoscale quantum devices[30]. Notable experiments that have shown such effects include transient grating experiments (with heat sources possessing characteristic dimensions of ~1–25 μm)[11,35–37], thermoreflectance-based pump-probe spectroscopy[15,17,32–34,38], and x-ray probing of stripline arrays[16,39]. One of the most notable aspects from all of these studies is the fact that non-diffusive transport is shown to result in considerably reduced thermal conductivities as compared to the bulk values of the various semiconducting materials.

Recently, studies have demonstrated that not only the size of the nanoscale heat sources, but the spacing between the heat sources can also significantly impact the thermal transport in the underlying layer[16,39–43]. More specifically, it has been observed that when the spacing between the heat sources were reduced to below the dominant heat-carrying phonon mean free paths, enhanced cooling of the underlying layer was achieved via collective diffusion. For instance, utilizing molecular dynamics (MD) simulations, Honarvar et al.[40] have shown up to ~13% increase in thermal conductance across thin silicon membranes with periodic nano-heater separations down to 1 nm.

In this work, we show that the thermal conductance across thin films can be enhanced by more than 7-fold through the strategic placement of not only periodic and closely spaced nano-heaters on top of the thin films, but the addition of tightly packed nano-coolers on the opposite ends. We attribute the dramatic enhancement in the cross-plane thermal conductance to the ability of the tightly packed nano-heaters/nano-coolers to efficiently 'funnel' the collective diffusion of phonons. Through extensive non-equilibrium molecular dynamics (NEMD) calculations, we show that the nano-heater/nano-cooler geometry for thin films promotes anharmonic scattering and limits phonon backscattering from the heat baths. We also show that introducing a thin region of atomic disorder at the film/heat bath interfaces can limit the specular phonon backscattering and further facilitate heat conduction across thin films. Thus, our systematic atomistic simulations show that contrary to the conventionally accepted notion of anharmonic phonon scattering leading to resistive pathways for heat conduction, the promotion of strategic anharmonic scattering via nano-heaters and nano-coolers resulting in the phonon 'funneling' effect can dramatically enhance thermal conduction across semiconductor thin films.

Results and discussions

We perform atomistic simulations of thin films based on Stillinger-Weber (SW) germanium with periodic nanostructures placed on top (nano-heaters) and bottom (nano-coolers). As shown in the schematic in Fig. 1a, these nanostructures with period P and a fixed duty cycle of 50% are placed on thin films with varying thicknesses of D ranging from 15 to 59 nm, to create steady-state temperature profiles that differ drastically from profiles resulting from conventional diffusive heat flow as we discuss in detail below.

The replacement of the uniform heat baths with nano-heaters and nano-coolers dramatically increases the effective cross-plane thermal

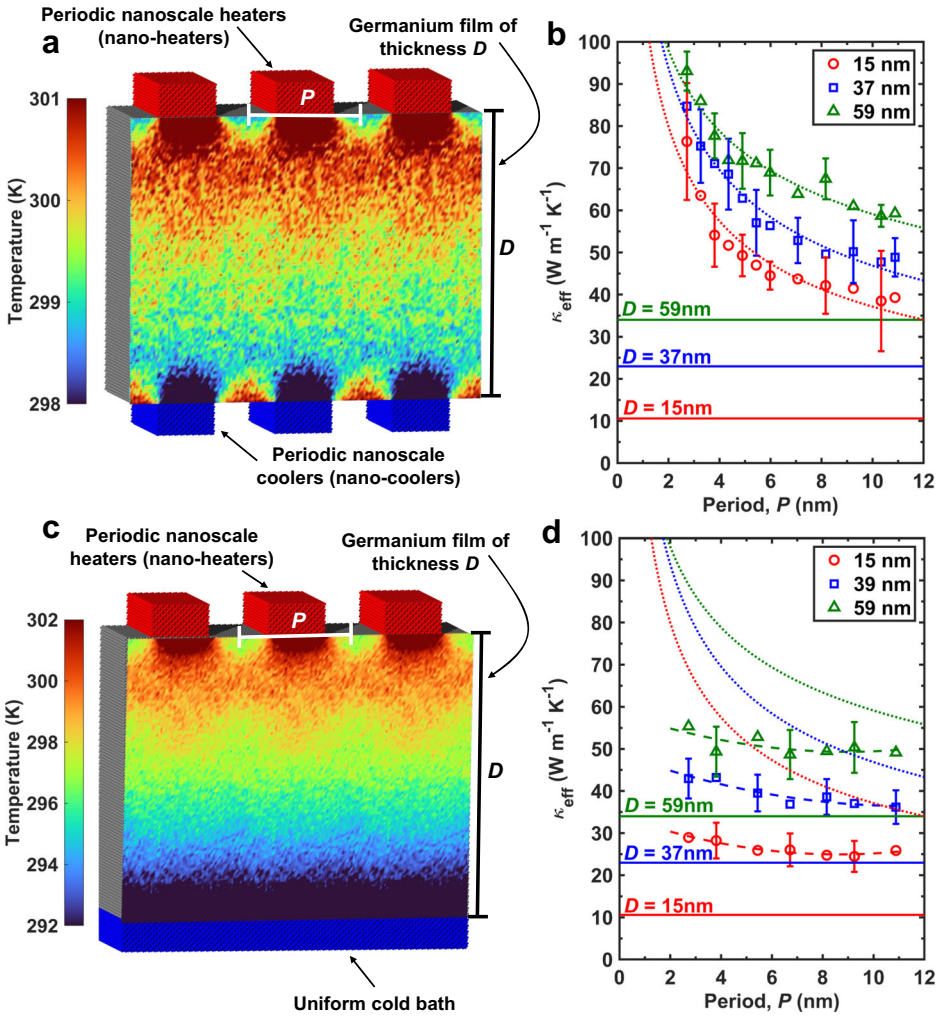

Fig. 1 | Enhancement in cross-plane thermal conductivity of germanium thin films by decreasing the period, *P*, of the nanoscale heat baths. a Schematic of our computational domain of germanium thin film with nano-heaters and nano-coolers attached on the top and bottom of the film, respectively. The color map shows the steady-state atomistic temperature profiles calculated from our non-equilibrium molecular dynamics simulations (NEMD). The thickness of the thin film (D) and the period of the nanostructured (P) heat sources and heat sinks were varied in our simulations. **b** The NEMD-calculated effective cross-plane thermal conductivities (κ_{eff}) of thin films with D = 15 nm, 37 nm and 59 nm are shown as a function of the period of the heat baths. For comparison, we also show the NEMD-predicted thermal conductivities of the thin films with uniform heat baths (solid lines). For the entire range of P studied in this work, κ_{eff} is dramatically enhanced for the films with the periodic heat sources and heat sinks as compared to films with the uniform heat baths. This increase in κ_{eff} is more pronounced at shorter P, with some values enhanced by more than 7-fold. **c** Schematic of our computational domain of germanium thin film with nano-heaters and a uniform heat sink attached on the top and bottom of the film, respectively. **d** As compared to the case with both the nano-heaters and nano-coolers, the enhancement in thermal conductivity for the case with just the nano-heaters is much less pronounced, especially at shorter periods. We attribute this to a more pronounced phonon `funneling' effect, as evident from the temperature profiles, for the case of the nano-heater/nano-cooler geometries, where phonons can efficiently carry heat across the thin films.

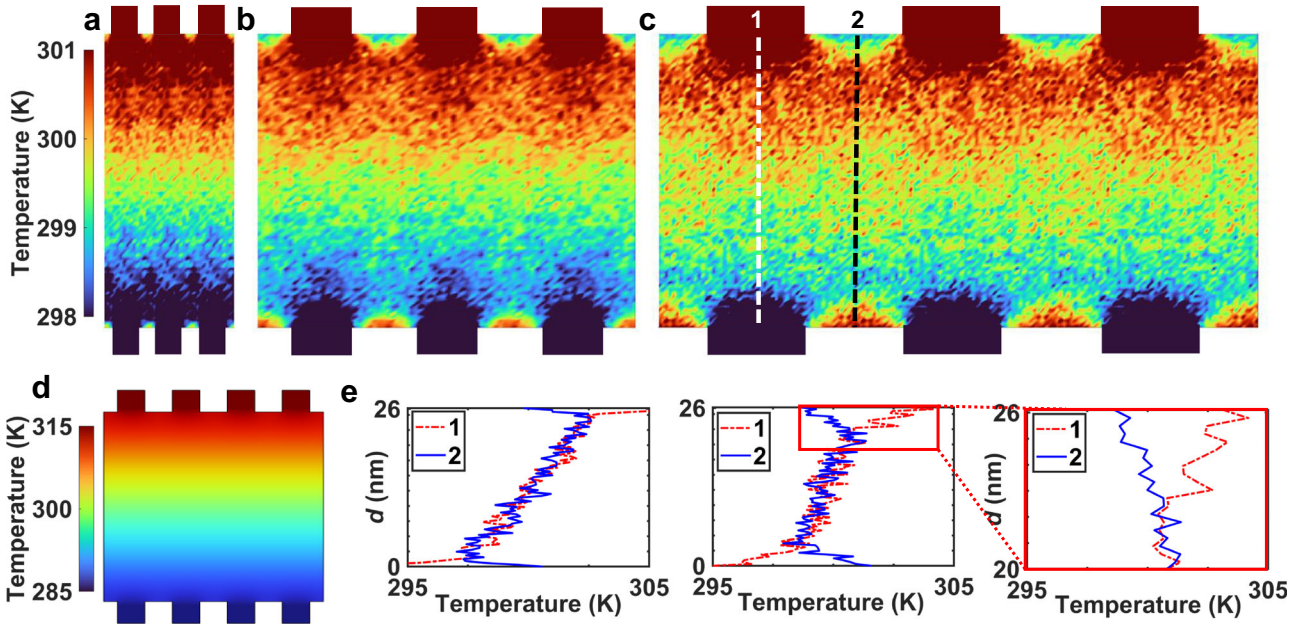

Fig. 2 | Non-diffusive temperature profiles of germanium thin films with nanoscale heat baths. Steady-state temperature profiles for our germanium thin films with thickness of 26 nm and with varying periods for the nanoscale heat baths of (**a**) 2.7 nm, (**b**) 5.4 nm, and (**c**) 10.9 nm. When compared to the temperature profile obtained from the diffusive model (based on the macroscopic Fourier's law) as shown in (**d**) for $P = 10.9$, the temperature profiles for films with the nanoscale heat baths show clear differences -- most prominently, the `light bulb'-shaped temperature profiles resulting from scattering of ballistic phonons originating from adjacent heat baths and the negative temperature gradients in the cross-plane direction as highlighted by region 2 in (**c**). **e** The area of the local regions adjacent to the heat baths with the negative temperature gradients are dictated by the period of the nanoscale heat sources and sinks and are more prominent for larger periods.

conductivities, κ_{eff}, of germanium thin films with the effect being enhanced at shorter periods as shown in Fig. 1b. Moreover, the increase in κ_{eff} at shorter periods of the nanoscale heat baths is larger for the thinnest germanium film ($D = 15$ nm) with almost 8× increase as compared to the 5× increase for the 59 nm thin film. As we observe the largest increase in the effective thermal conductivity for our thinnest (15 nm) film, this could be attributed to the phonon wavelength spectrum in the range of 1–15 nm of the bulk phonon spectrum in germanium. In this regard, lattice dynamics calculations from Landry and McGaughey have shown that the mean free path spectrum of phonons in SW germanium can span a wide range (of more than three orders of magnitude)[44]. Their calculations showed that the average phonon mean free path of $\lesssim$27 nm contributed 51% to the thermal conduction when phonon transport is ballistic. Considering this, at the length scales of our thinnest film (15 nm), the wavelength of phonons emitted from the nano-heaters might have been altered due to phonon confinement effects, and as such, the interpretation of our results in terms of the bulk phonon properties might not be valid. Moreover, although the DOS of atoms at the center of the thin film (sufficiently away from the nanoscale heat baths) is similar to that of the 'bulk' germanium (see Supplementary Fig. 7), the contributions to heat conduction from the spectrum of phonons being emitted by the nanoscale heat baths might be very different than that in bulk. However, analyzing such phonon confinement effects is beyond the scope of the current work, but deserves further investigation.

For our germanium thin films, we also conduct additional simulations with nano-heaters attached at the top and a uniform cold bath on the bottom of the films as shown in Fig. 1c, d. We note that the temperature range in Fig. 1c differs from that in Fig. 1a in order to qualitatively compare the temperature fields between the two cases. In both cases, an identical amount of heat is added/subtracted from the heat baths (more details are given in the Methods section). While this nano-heater/uniform heat bath configuration also leads to higher κ_{eff} as compared to the uniform heat source and heat sink cases, the increase is considerably lower when compared to the cases with both the nano-heaters and nano-coolers, especially at shorter periods. Additionally, κ_{eff} of germanium films with only the nano-heaters on top (and a uniform heat sink at the bottom) are significantly less dependent on the period of the nano-heaters, as opposed to the strong period dependence for thin films with the nano-heater/nano-cooler geometry. This shows that replacing the uniform heat sinks with nano-coolers can increase heat conduction by more than twice that of thin films with just the nano-heaters, especially for shorter periods, thus providing an efficient knob with a larger control over the thermal transport across semiconducting thin films.

We ascribe the increase in the effective cross-plane heat conduction of our thin films with the nanoscale heat baths partly to the efficient 'funneling' of phonons in the direction of the applied heat flux as represented in Fig. 1a from our atomistic temperature profiles (see the Computational Methods for details of the calculations). We also ascribe the increase partly to the reduction in the specular back-reflection of phonons from the heat baths that otherwise provides a strong resistance to cross-plane heat conduction in thin films with the uniform heat sources and heat sinks. In what follows, we will provide evidence to support these phenomena with a deeper understanding of phonon 'funneling'. Note, as we cannot separate the scattering that occurs at the heat bath/film interface (due to the vibrational mismatch as shown in the Supplementary Fig. 18) and the scattering that occurs at the fixed wall boundaries, we have lumped these two scattering mechanisms as scattering that occurs at the heat baths.

The mechanism which we refer to as 'phonon funneling' is best represented with temperature profiles for our computational domains with varying periods of the nanoscale heat baths (Fig. 2a–c). We observe 'light bulb'-shaped temperature profiles originating from both the nano-heaters and nano-coolers, the shape of which depends on how closely the adjacent heat baths are packed together. This is drastically different than the diffusive temperature profiles calculated from finite-element analysis simulations that utilize Fourier's law of heat conduction (even with the nanostructured heat baths as shown for the case of $P = 10.9$ nm in Fig. 2d). Moreover, contrary to the diffusive picture, we observe negative temperature gradients in local regions adjacent to the nano-heaters and nano-coolers (region '2' in Fig. 2c) that are more pronounced for domains with larger periods as shown in Fig. 2e. This has been recently observed in experiments and also shown through computations, where similar negative temperature gradients were

ascribed to the ballistic nature of phonons[13,39,40,45]. When ballistic transport dominates, energy is deposited non-locally, and phonons with mean free paths longer than the period, and originating from adjacent nano-heaters at the top of the film, traverse ballistically and scatter midway between the heaters, thus forming the 'light bulb'-shaped temperature profiles. At the bottom of the film, preferential phonon scattering at the free surfaces near the nano-coolers leads to local regions with higher temperatures, thus facilitating the 'phonon funneling' phenomena, where the vibrations are guided towards the periodic heat sinks (as clearly observed from our temperature profile calculations near the nano-coolers). Thus, such preferential scattering of phonons via interactions of ballistic phonons from adjacent nano-heaters and phonon-boundary scattering at the free surfaces adjacent to the nano-coolers lead to higher κ_{eff} as compared to the thin films with uniform heat baths (Fig. 1d). A schematic diagram of this mechanism is shown in Fig. 3. This 'phonon funneling' phenomenon is similar to the 'directional thermal channeling' as proposed by Honarvar et al.[40], in which strategic scattering near nanostructured heat baths led to the channeling of heat in the through-plane direction of silicon thin films with a uniform heat sink. In our case, along with this 'directional thermal channeling' that is introduced through phonon scattering near the nano-heaters, we also introduce additional phonon scattering near the nano-coolers to guide phonons into the nano-coolers, thereby efficiently 'funneling' heat across the thin films and drastically enhancing the effective thin film thermal conductivities; note, while Honarvar et al.[40] report a modest increase in the thermal conductivity of thin films through the directional thermal channeling effect, our calculations show that the nano-heater/nano-cooler geometry can result in as much as 8× increase in the effective thermal conductivity of thin films through the 'phonon funneling' effect in our SW germanium thin films. It is also interesting to note that we calculate similar thermal conductivities for thin films with either nano-heater/uniform heat sink or with uniform heat source/nano-cooler geometries (see Supplementary Fig. 3), which suggests that the scattering occuring near the nano-coolers and nano-heaters are also similar in nature. The combination of such scattering processes leads to the 'phonon funneling' phenomenon which drastically enhances the cross-plane thermal conductivity of the thin films. Considering our results for films with the nanoscale heat baths as compared to the cases with the conventional uniform heat baths, we conjecture that considerable ballistic phonon scattering at the heat baths leads to specular phonon backscattering from the free surfaces on top/bottom of the heaters/coolers, ultimately resulting in the comparatively higher resistances to heat flow in films with uniform heat baths.

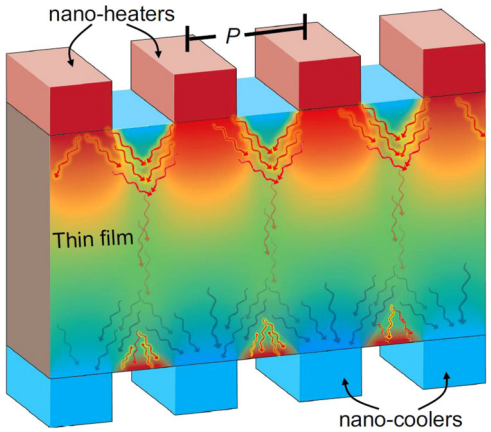

Fig. 3 | Schematic diagram of the phonon funneling mechanism. Scattering of phonons from adjacent closely packed nano-heaters channels phonons across the thin film. Preferential scattering of phonons at the free surfaces between closely packed nano-coolers (resulting in regions of higher temperature), facilitates the `funneling' of phonons into the nano-coolers.

To understand the phonon scattering mechanisms dictating the effective cross-plane thermal conductivities of our germanium thin films, we first compare the temperature-dependent thermal conductivities (κ_{eff}(T)) for the different geometries in Fig. 4a. The temperature-dependent trends can provide insight into the level of anharmonicity within the system and also elucidate the level of ballistic transport occurring within the system. For instance, in pure crystals, the lattice thermal conductivity dependence on temperature typically demonstrates a ~1/T trend, driven by anharmonic (Umklapp) scattering involving three-phonon processes[46–48]. However, if ballistic transport dominates and the thin film thermal conductivity is dictated mainly via boundary scattering of these ballistic phonons, κ_{eff}(T) demonstrates a much reduced temperature dependence at intermediate temperatures[49–52], (barring quantum effects). Figure 4a compares κ_{eff}(T) for our thin films with the nano-heater/nano-cooler configuration with P = 3.3 nm and 10.9 nm and a thickness of D = 26 nm. For comparison, we also show the thermal conductivity of a 26 nm film with just the nano-heaters at P = 3.3 nm (and with a uniform heat sink). As is clear from the temperature dependencies shown in Fig. 4a, a combination of anharmonic scattering and ballistic phonon scattering at the boundaries dictate the thermal conductivity of these thin films. However, anharmonic scattering plays a more dominant role for thin films with both the nano-heater/nano-cooler configurations, especially when the nanoscale heat baths have shorter periods. This enhanced anharmonicity supports the claim of increased phonon-phonon scattering from close-packed nanoscale heat baths resulting in increased κ_{eff}(T) at intermediate temperatures. Furthermore, the greater temperature dependency of the film with the nano-coolers as compared to the film with the uniform heat sink suggests that limiting

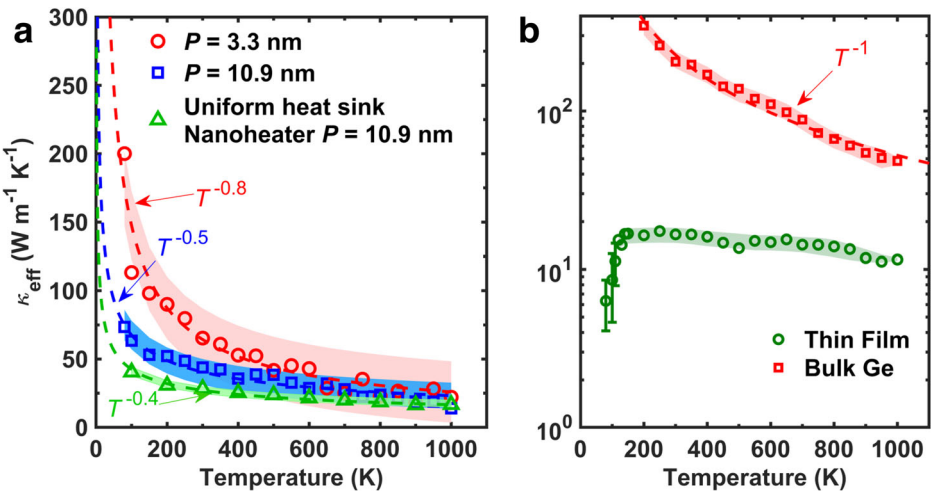

Fig. 4 | Temperature-dependent cross-plane thermal conductivities of thin films with and without the nanoscale heat baths. a Temperature dependence of the effective cross-plane thermal conductivities for our germanium thin films with 26 nm thickness and periods, P, of 3.3 nm and 10.9 nm for the nano-heaters and nano-coolers attached on top and bottom of the films, respectively. For comparison, we also plot the temperature-dependent thermal conductivity of 26 nm thick germanium film with a uniform heat sink attached on the bottom and P = 3.3 nm for nano-heaters attached on the top. **b** κ_{eff}(T) for 26 nm germanium thin film with uniform heat baths and Green-Kubo thermal conductivity predictions of bulk germanium.

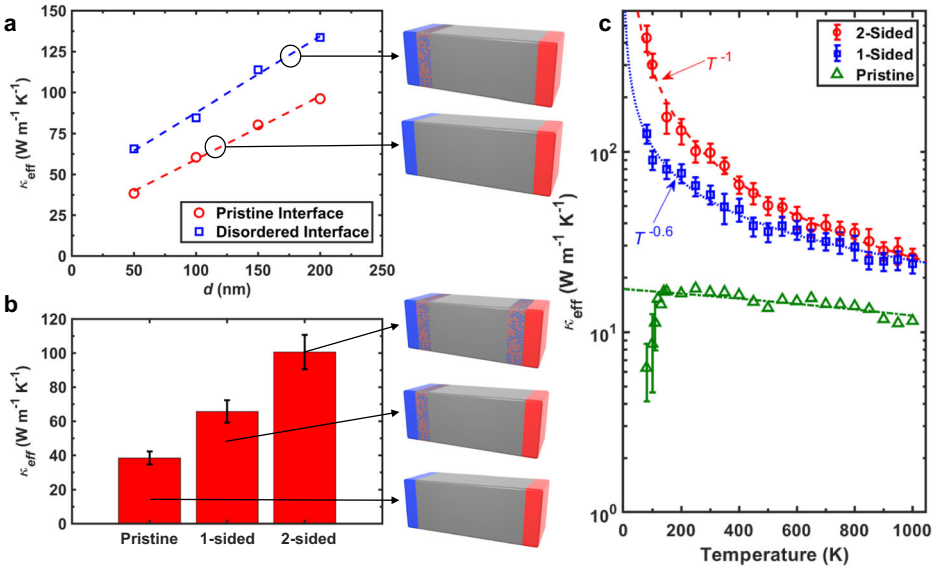

Fig. 5 | Enhancing cross-plane thermal conductivity through specular phonon reflections at the heat baths and limiting phonon backscattering. a Comparison of effective cross-plane thermal conductivities as a function of film thickness for germanium thin films with pristine interfaces between the film/uniform heat baths and films with a thin (~ 2 nm thick 50/50 Si/Ge random alloy) disordered region near the heat sink. The disordered region prevents specular backscattering of higher frequency phonons and enhances κ_{eff} for the entire range of thin film thicknesses. **b** κ_{eff} is enhanced even more when the disordered region is present near both the heat sink and heat source. **c** The disordered regions drastically change the temperature dependence when compared to thin films with pristine interfaces near the baths. Limiting the specular backscattering of higher frequency phonons from the heat baths results in enhanced anharmonicities and better heat conduction across the thin films.

specular phonon backscattering from the heat baths can promote anharmonic energy exchange between the phonons in the thin films.

To emphasize the role of specular phonon backscattering from the heat baths, in Fig. 4b we compare κ_{eff}(T) of our 26 nm germanium thin film with uniform heat baths with κ_{eff}(T) for bulk germanium calculated from our additional Green-Kubo simulations (details in the Supplementary Information). The drastically varying temperature trends suggest completely different phonon scattering mechanisms in the two cases; while three-phonon anharmonic processes dictate the thermal conductivity of bulk germanium (as evident from the ~1/T trend), predominant boundary scattering in the case of our thin film with uniform heat baths leads to the increasing thermal conductivity with temperature for the low temperature (< 200 K) range following a temperature-independent thermal conductivity at relatively higher temperatures. It is worth noting that the temperature dependence for the uniform heat bath case is completely different to the temperature trend for our thin films with the nanoscale heat baths, where the thermal conductivity at low temperature increases due to the reduction in the resistive phonon-phonon scattering processes. The decrease in κ_{eff}(T) at very low temperatures for the thin film with uniform heat baths can be ascribed to the enhancement in phonon backscattering at the heat baths without the thermalizing anharmonic processes for the relatively higher frequency phonons. These anharmonic processes for the higher frequencies are inherently more prevalent at higher temperatures. The key difference here between the film with the nanoscale heat baths and the film with the uniform heat baths is that anharmonic scattering in the former leads to the efficient 'funneling' of phonons from the nanoscale heat source to the heat sink, thus facilitating heat conduction. Whereas, in the later, it would predominantly act to thermalize the phonons that are backscattered from the heat baths - in the absence of which, the cross-plane thermal conductivity decreases at low temperatures as shown in Fig. 4b.

To further investigate our conjecture that specular backscattering of the higher frequency phonons from the heat baths is driving the reduction in thermal conductivity for the films with uniform baths, we run additional simulations where we introduce a very thin region (of ~2 nm) of a 50–50 silicon-germanium random alloy near the baths to create disorder near the interfaces leading to diffuse scattering of higher frequency phonons and thus limiting their specular backscattering. Figure 5a shows the κ_{eff} of our germanium thin films with uniform baths compared to the case with the disordered alloy region near the cold bath as a function of film thickness, D, in the range of 50 to 200 nm. As is clear, the disordered region leads to a higher cross-plane heat conduction across the entire range of thin film thicknesses. Moreover, creating disordered regions near both the hot and cold baths leads to substantially higher κ_{eff}(T) as shown in Fig. 5b for the case of D = 150 nm. The increase in thermal conductivity with the disordered regions suggests that thermalizing events from the diffuse phonon-disorder scattering reduces the specular backscattering of higher frequency phonons from the heat baths leading to substantially higher heat conduction across the thin film. It is important to note that only the higher frequency phonons in the spectrum can scatter at the thin disordered region and lower frequency (longer wavelength) phonons can transmit across the thin disordered region without energy loss as confirmed by our additional wave-packet simulations shown in the Supplementary Fig. 10, where we launch longitudinal phonons with different frequencies and calculate their transmission across the thin disordered region.

In this regard, recent prior works have shown that disordered or rough interfaces can enhance thermal boundary conductance[53–57]. In particular, Liang et al.[53,54] have shown that ballistic transport in thin films coupled with specular scattering at film/substrate interfaces can result in phonons returning to the substrate without energy transfer in the films, thus leading to higher interfacial resistances. Although we are not concerned with interfacial energy transfer in this study, the reduction in specular scattering at the film/bath interfaces, similar to Liang et al.'s[53,54] observations, allows phonons to transfer their energy more efficiently in the cross-plane direction, thus leading to higher κ_{eff}. We note that although long wavelength phonons directly scatter at the heat baths and do not facilitate the heat transfer[8,58], our results show that the reduction in the specular scattering of shorter wavelength (higher frequency) phonons (that are scattered at the disordered region) near the heat baths can dramatically enhance the effective cross-plane thermal conductivities of thin films. In other words, the diffuse scattering of these short wavelength phonons at the heat baths leads to better energy transfer across the thin films and reduction in the cross-plane resistive pathways that would otherwise, for films with pristine interfaces, facilitate phonon backscattering at the heat baths leading to reduced κ_{eff}.

This diffuse scattering at the interfacial region for the thin films with the local disorder also leads to increased anharmonicity (and better energy coupling between different phonon modes) as evidenced from the ~1/T trend in their temperature-dependent κ_{eff}(T) (Fig. 5c). Compared to the temperature dependence of the thin film with the pristine interface, this drastically different temperature trend further suggests that increased anharmonic interactions leading to better energy transfer in the thin films can be facilitated through the diffuse scattering of phonons at the disordered film/heat bath interfaces.

A similar effect of enhanced cross-plane thermal conductivity for thin films could also be realized with the addition of geometric roughness where

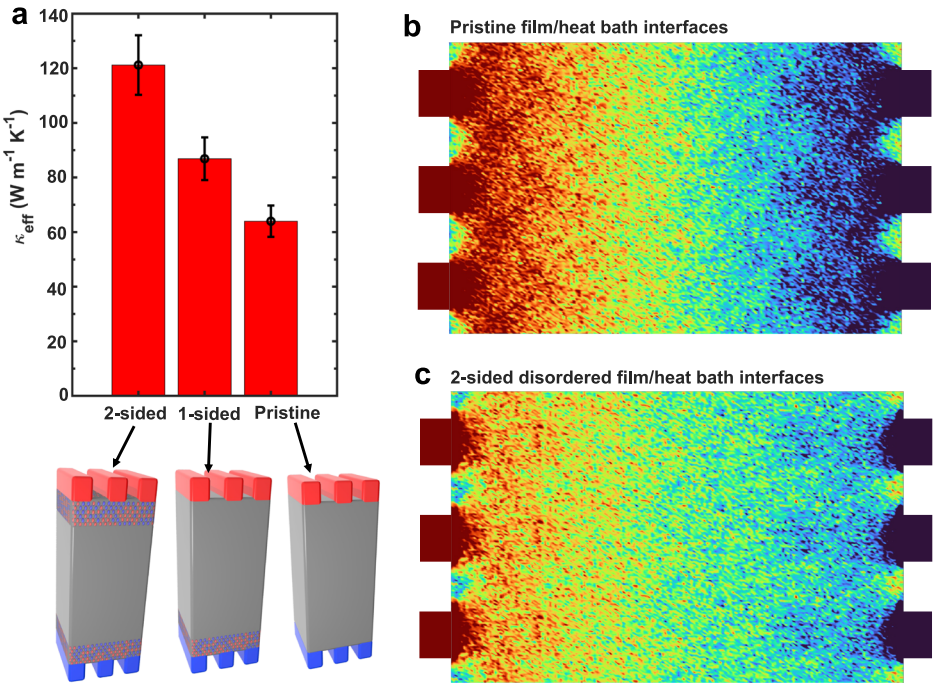

Fig. 6 | Effect of added disorder at the thin film boundaries on the non-diffusive heat transfer in thin films with periodic nanoscale heat baths. **a** The introduction of disordered regions near the nanostructured heat baths can further increase the κ_{eff} of thin films by limiting specular backscattering of phonons. **b** As evident from the steady-state temperature profiles, the disordered regions can reduce the `light bulb' effect from quasi-ballistic phonon scattering and limit the phonon `funneling' effect, the reduction in phonon backscattering outweighs this effect and results in higher κ_{eff}, thus providing an additional knob to enhance cross-plane heat conduction in semiconductor thin films.

atomic species are varied or removed depending on the geometric region at the surfaces to emulate 'rough' surfaces[59,60]. However, to fully understand the influence of such geometric roughness, where it could be expected that short-wavelength phonons are diffusely scattered while longer wavelengths are specularly scattered depending on the length scale of the rough surfaces, requires a more dedicated study. As such, although systematically varying surface roughness across a wide length scale is beyond the scope of the current work, we believe this requires a more detailed study so as to fully unravel the potential of phonon boundary scattering to efficiently enhance the thermal conductivity of thin films.

We note that the mechanism driving this increase in thermal conductivity is very different than the one in our nanoscale heat bath cases; while anharmonic scattering of ballistic phonons facilitated by the nanoscale baths, as evident from the temperature dependence of thermal conductivity shown in Fig. 4, leads to the 'funneling' of phonons from the hot to the cold baths (as also evident from our atomistic temperature profiles in Fig. 2a–c), the diffuse scattering at the disordered region does not facilitate such 'funneling' effects. However, when both of these mechanisms are combined, κ_{eff} can be enhanced further as shown in Fig. 6a. Although the alloyed disordered regions near the heat baths disrupt the funneling effect to some extent, as suggested by our atomistic temperature profiles of the different domains shown in Fig. 6b, c, where the 'light bulb' shapes are considerably diminished due to higher frequency phonon scattering at the alloy regions, it still augments cross-plane heat conduction by limiting specular phonon backscattering from the heat baths.

We also performed additional simulations in which we vary the height of the nanoscale heat baths without adding a disordered region within the thin films. The effective thermal conductivities are shown in the Supplementary Fig. 5 for a 26 nm film with nanoscale heat baths with varying heights of 1–12 nm (and P = 5.44 nm). Note, for the results presented above, we have kept the height of the nanoscale heat baths fixed at 3 nm. As the height of the nanoscale heat baths is increased, the effective thermal conductivity of the thin films also increases but plateaus at a bath height of ~9 nm. This could be due to enhanced phonon scattering at these longer heat baths, further reducing specular backscattering from these regions and resulting in a larger effective thin film thermal conductivity. However, even for small heat bath heights (<3 nm), the effective thin film thermal conductivity is substantially increased over the case with uniform heat baths, signifying a strong role of the phonon 'funneling' phenomenon in thin films with periodic nano-heaters/coolers. Moreover, we calculate the DOS of atoms within the 3 nm and 12 nm heat bath, as shown in the Supplementary Fig. 18 of the Supplementary Information. A 'liquid-like' DOS is observed along with a significant vibrational mismatch between the heat baths and the thin film which differs for the 3 nm and 12 nm heat bath. Note, liquids demonstrate a large peak in the DOS at low frequencies, which are distinctly different from the vibrational DOS of solids (see Supplementary Fig. 7 of the Supplementary Information)[61]. This mismatch could lead to varying strengths of phonon scattering at the heat bath/film interface, resulting in a higher effective thermal conductivity for films with longer heat baths.

To summarize our findings on the strategies to significantly enhance the cross-plane thermal conductivity of semiconductor thin films: (i) uniform heat baths can be replaced with nano-heaters and nano-coolers to increase anharmonic scattering from the interaction of ballistic phonons originating from adjacent heat baths leading to the 'light-bulb'-shaped temperature profiles. (ii) This leads to the efficient 'funneling' of phonons in the cross-plane direction and also limits specular phonon backscattering from the film/heat bath interfaces. (iii) These effects are more pronounced for tightly packed nano-heaters/nano-coolers resulting in larger temperature dependencies of the cross-plane thermal conductivities, thus supporting the notion of increased anharmonicities leading to the efficient funneling of heat-carrying phonons from the nano-heaters to the nano-coolers. (iv) Introducing disorder and thus facilitating diffuse scattering of higher frequency phonons by limiting their specular backscattering at the film/heat bath interfaces can further enhance the cross-plane heat conduction in thin films. Therefore, the strategic scattering of phonons by combining diffuse film/heat bath interfaces along with the placement of nano-heaters/nano-coolers that facilitate the quasi-ballistic effect leading to efficient phonon 'funneling' can be utilized to drastically enhance the effective cross-plane thermal conductivities of semiconductor thin films.

Methods

To investigate the thermal properties of our semiconductor thin films, we conducted systematic atomistic simulations on silicon and germanium thin films with the addition of nanoscale heat baths placed on either end of the thin film. An example structure with attached nanoscale heat baths is shown in the Supplementary Fig. 1a, where the period, P, and the film thickness, D

are varied. In all cases, the width of each nanostructure is half of the period length. For all of our simulations, we use the Large-scale Atomic/Molecular Massively Parallel Simulator (LAMMPS) package[62]. We used the Stillinger-Weber (SW) potential[63] to model the interatomic interactions of both the silicon and germanium systems. The SW potential has been widely used in prior literature to study the thermal and mechanical properties of similar systems[64–68]. After creating our structures, we perform an energy minimization with stopping tolerances of 1×10^{-4} and 1×10^{-6} for the energy and force, respectively. After minimization, we raise the temperature of the system from 0 to 300 K under the *N-P-T* ensemble (constant number of atoms, pressure, and temperature) for 0.5 ns, and further equilibrate at 300 K under the *N-P-T* ensemble for an additional 1 ns. Afterwards, we switch to the *N-V-T* ensemble (constant number of atoms, volume, and temperature) for an additional 1 ns. For all simulations, we use a timestep of 1 fs. The total number of atoms within our simulations varies between ~71,000 to ~800,000 atoms depending on the nano-heater/nano-cooler period and film thickness. In all cases, the total number of nano-heater/nano-cooler periods is kept constant.

To determine the thermal conductivity of our thin films, we utilize the non-equilibrium molecular dynamics (NEMD) approach to directly calculate the effective thin film thermal conductivity via Fourier's law, given by,

$$q'' = -\kappa \frac{dT}{dx} \tag{1}$$

where q'' is the applied heat flux, κ is the effective thin film thermal conductivity, and $\frac{dT}{dx}$ is the temperature gradient across the thin film between nanostructures in the direction of the applied heat flux. In this technique, hot and cold baths are placed on either end of the simulation domain where energy is added or subtracted from groups of atoms, establishing a temperature gradient across the domain as shown in the Supplementary Fig. 1b. On either end of the domain, a unit-cell thick layer of atoms is fixed and does not interact with the other atoms within the system. In this way, heat flows from the hot bath to the cold bath through the length of the system, as opposed to flowing across the periodic boundaries adjacent to the heat baths[54,69–72]. The atoms within the thin film are binned into 100 equally spaced bins along the *x*-direction (which is the direction of the applied heat flux), yielding ~ 800–8000 atoms in each bin, depending on the nano-heater/nano-cooler period and film thickness. In each bin, atomic temperatures are averaged along the *y*- and *z*-directions, yielding a 1D temperature gradient for the calculation of the effective thin film thermal conductivity. In this way, the temperature anomalies (e.g. the 'lightbulb' shapes near the nano-heaters/nano-coolers) are averaged out. It is important to note that in our NEMD simulations to calculate the effective cross-plane thermal conductivities, we do not simply take the temperature gradient along a line connecting nano-heater center to nano-cooler center, but rather the temperature gradient averaged over the in-plane direction of the film. In doing so, we assume that the heat flux along the *x*-direction is equivalent to the heat that is added/subtracted from the heat baths due to the periodic nature of the simulations along the *y*- and *z*-directions. In order to verify this assumption, we have calculated the heat flux at different lateral locations and obtained the same values, as shown in the Supplementary Fig. 16 (further details of these calculations can be found in the Supplementary Information). Moreover, we calculate the effective cross-plane thermal conductivities of the thin films by considering the central portion of the temperature gradient away from the nano-heaters/nano-coolers, as has been the standard approach in NEMD simulations[54,69–72]. This is primarily to reduce uncertainties from the non-linear temperature profiles near the baths when calculating the thermal conductivity by invoking Fourier's law[54,69–72]. However, since our 1D temperature profiles are linear throughout the entire thickness of the thin films (because we average out the 'light-bulb' shaped temperature anomalies near the periodic heat baths), fitting the temperature profiles even beyond the central region does not lead to significant differences in our predicted thermal conductivites (see Supplementary Fig. 17).

After equilibration, we activate our heat baths by adding/subtracting 3 eV ps^{-1} of energy from the hot and cold baths, respectively, using the *fix heat* command in LAMMPS for a total of 3 ns to establish a temperature gradient. After a gradient has been established, we average atomic temperatures within each bin for an additional 2 ns to extract our 1D temperature gradient in order to calculate the effective thin film thermal conductivity. It has been shown that the *fix heat* command in LAMMPS exhibits an energy drift over long simulation times. However, we carefully monitor the energy of our system during the data collection run to ensure that energy is properly conserved throughout this period. Additionally, we have performed additional simulations using the *fix ehex* command (which performs better with regards to energy drifts during the simulations) and obtained similar results to using the *fix heat* command ($\kappa_{eff} = 51.2$ and 49.1 W m^{-1} K^{-1} for *fix heat* and *fix ehex*, respectively for a 26 nm thin film with attached nano-heaters/coolers with $P = 5.4$ nm).

Typically, in order to calculate the thermal conductivity of a bulk material via the NEMD approach, simulations of increasing size along the direction of the applied heat flux are conducted and a linear extrapolation of $1/\kappa$ vs. $1/L$ is performed to approximate κ as $L \rightarrow \infty$[64,69,73]. This is due to the need to capture the dominant heat carriers within the system, as phonons with wavelengths longer than the domain length will predominantly scatter at the baths and not contribute significantly to the overall thermal conductivity. However, in our simulations, we are interested in the thermal conductivity of a thin film with a specific thickness rather than the thermal conductivity of the corresponding bulk material.

We also visualize the temperature profiles of our systems through the calculation of individual atomic kinetic energies. This approach to calculate and visualize the temperature profiles is based on the method that was originally utilized by Honarvar et al. to visualize their temperature fields for similar SW silicon-based computational domains with nano-heaters and uniform heat sinks[40]. The system is subdivided into a number of bins in the *x*- and *z*- directions, and the kinetic energy of each atom within each bin is averaged across the *y*-direction for all atoms in that bin. The temperature of each bin is then calculated by,

$$T_i = \frac{2E_i}{3k_b} \tag{2}$$

where T_i and E_i is the average temperature and average kinetic energy of the *i*th bin, respectively, and k_b is the Boltzmann constant. In such a way, the two dimensional visualization of the temperature profile is calculated for our thin films.

Data availability

The data supporting the present work are available from the corresponding authors upon reasonable request.

Received: 7 December 2023; Accepted: 26 July 2024;
Published online: 12 August 2024

References

1. Lee, J.-H., Galli, G. A. & Grossman, J. C. Nanoporous Si as an efficient thermoelectric material. *Nano Lett.* **8**, 3750–3754 (2008).
2. Wang, Y. et al. Phonon lateral confinement enables thermal rectification in asymmetric single-material nanostructures. *Nano Lett.* **14**, 592–596 (2014).
3. Loke, D., Skelton, J. M., Chong, T.-C. & Elliott, S. R. Design of a nanoscale, CMOS-integrable, thermal-guiding structure for boolean-logic and neuromorphic computation. *ACS Appl. Mater. Interfaces* **8**, 34530–34536 (2016).
4. Pop, E. Energy dissipation and transport in nanoscale devices. *Nano Res.* **3**, 147–169 (2010).
5. Cahill, D. G. et al. Nanoscale thermal transport. II. 2003–2012. *Appl. Phys. Rev.* **1**, 011305 (2014).

6. Moore, A. L. & Shi, L. Emerging challenges and materials for thermal management of electronics. *Mater. Today* **17**, 163 – 174 (2014).
7. Warzoha, R. J. et al. Applications and impacts of nanoscale thermal transport in electronics packaging. *J. Electron. Packaging* **143**, 020804 (2021).
8. Majumdar, A. Microscale heat conduction in dielectric thin films. *J. Heat. Transf.* **115**, 7–16 (1993).
9. Chen, G. Non-Fourier phonon heat conduction at the microscale and nanoscale. *Nat. Rev. Phys.* **3**, 555–569 (2021).
10. Esfarjani, K., Chen, G. & Stokes, H. T. Heat transport in silicon from first-principles calculations. *Phys. Rev. B* **84**, 085204 (2011).
11. Johnson, J. A. et al. Direct measurement of room-temperature nondiffusive thermal transport over micron distances in a silicon membrane. *Phys. Rev. Lett.* **110**, 025901 (2013).
12. Chen, G. Nonlocal and nonequilibrium heat conduction in the vicinity of nanoparticles. *J. Heat. Transf.* **118**, 539–545 (1996).
13. Yang, R. & Chen, G. Thermal conductivity modeling of periodic two-dimensional nanocomposites. *Phys. Rev. B* **69**, 195316 (2004).
14. Cahill, D. et al. Nanoscale thermal transport. *J. Appl. Phys.* **93**, 793–818 (2003).
15. Regner, K. T. et al. Broadband phonon mean free path contributions to thermal conductivity measured using frequency domain thermoreflectance. *Nat. Commun.* **4**, 1640 EP – (2013).
16. Siemens, M. E. et al. Quasi-ballistic thermal transport from nanoscale interfaces observed using ultrafast coherent soft X-ray beams. *Nat. Mater.* **9**, 26–30 (2010).
17. Minnich, A. J. et al. Thermal conductivity spectroscopy technique to measure phonon mean free paths. *Phys. Rev. Lett.* **107**, 095901 (2011).
18. Koh, Y. K., Cahill, D. G. & Sun, B. Nonlocal theory for heat transport at high frequencies. *Phys. Rev. B* **90**, 205412 (2014).
19. Chen, G. Ballistic-diffusive heat-conduction equations. *Phys. Rev. Lett.* **86**, 2297–2300 (2001).
20. Sadasivam, S., Chan, M. K. Y. & Darancet, P. Theory of thermal relaxation of electrons in semiconductors. *Phys. Rev. Lett.* **119**, 136602 (2017).
21. Vermeersch, B. Compact stochastic models for multidimensional quasiballistic thermal transport. *J. Appl. Phys.* **120**, 175102 (2016).
22. Vermeersch, B., Mohammed, A. M. S., Pernot, G., Koh, Y. R. & Shakouri, A. Superdiffusive heat conduction in semiconductor alloys. II. Truncated Levy formalism for experimental analysis. *Phys. Rev. B* **91**, 085203 (2015).
23. Vallabhaneni, A. K., Singh, D., Bao, H., Murthy, J. & Ruan, X. Reliability of Raman measurements of thermal conductivity of single-layer graphene due to selective electron-phonon coupling: a first-principles study. *Phys. Rev. B* **93**, 125432 (2016).
24. Hua, C. & Minnich, A. J. Analytical Green's function of the multidimensional frequency-dependent phonon Boltzmann equation. *Phys. Rev. B* **90**, 214306 (2014).
25. Zobeiri, H., Hunter, N., Wang, R., Wang, T. & Wang, X. Direct characterization of thermal nonequilibrium between optical and acoustic phonons in graphene paper under photon excitation. *Adv. Sci.* **8**, 2004712 (2021).
26. Vermeersch, B., Carrete, J., Mingo, N. & Shakouri, A. Superdiffusive heat conduction in semiconductor alloys. I. Theoretical foundations. *Phys. Rev. B* **91**, 085202 (2015).
27. Mohammed, A. M. S. et al. Fractal Lévy heat transport in nanoparticle embedded semiconductor alloys. *Nano Lett.* **15**, 4269–4273 (2015).
28. -C. Hua, Y., -L. Li, H. & -Y. Cao, B. Thermal spreading resistance in ballistic-diffusive regime for GaN HEMTs. *IEEE Trans. Electron Devices* **66**, 3296–3301 (2019).
29. Zhao, Y. et al. Thermal transport in 2D semiconductors—considerations for device applications. *Adv. Funct. Mater.* **30**, 1903929 (2020).
30. Vanacore, G. M. et al. Diffraction of quantum dots reveals nanoscale ultrafast energy localization. *Nano Lett.* **14**, 6148–6154 (2014).
31. Shakouri, A. Nanoscale thermal transport and microrefrigerators on a chip. *Proc. IEEE* **94**, 1613–1638 (2006).
32. Wilson, R. B. & Cahill, D. G. Anisotropic failure of Fourier theory in time-domain thermoreflectance experiments. *Nat. Commun.* **5**, 5075 (2014).
33. Koh, Y. K. & Cahill, D. G. Frequency dependence of the thermal conductivity of semiconductor alloys. *Phys. Rev. B* **76**, 075207 (2007).
34. Wilson, R. B. & Cahill, D. G. Limits to Fourier theory in high thermal conductivity single crystals. *Appl. Phys. Lett.* **107** (20) https://doi.org/10.1063/1.4935987 (2015).
35. Johnson, J. A. et al. Phase-controlled, heterodyne laser-induced transient grating measurements of thermal transport properties in opaque material. *J. Appl. Phys.* **111**, 023503 (2012).
36. Johnson, J. A., Eliason, J. K., Maznev, A. A., Luo, T. & Nelson, K. A. Non-diffusive thermal transport in GaAs at micron length scales. *J. Appl. Phys.* **118**, https://doi.org/10.1063/1.4933285 (2015).
37. Huberman, S. et al. Unifying first-principles theoretical predictions and experimental measurements of size effects in thermal transport in SiGe alloys. *Phys. Rev. Mater.* **1**, 054601 (2017).
38. Highland, M. et al. Ballistic-phonon heat conduction at the nanoscale as revealed by time-resolved x-ray diffraction and time-domain thermoreflectance. *Phys. Rev. B* **76**, 075337 (2007).
39. Hoogeboom-Pot, K. M. et al. A new regime of nanoscale thermal transport: collective diffusion increases dissipation efficiency. *Proc. Natl Acad. Sci.* **112**, 4846–4851 (2015).
40. Honarvar, H. et al. Directional thermal channeling: a phenomenon triggered by tight packing of heat sources. *Proc. Natl Acad. Sci.* **118**, e2109056118 (2021).
41. Chen, X., Hua, C., Zhang, H., Ravichandran, N. K. & Minnich, A. J. Quasiballistic thermal transport from nanoscale heaters and the role of the spatial frequency. *Phys. Rev. Appl.* **10**, 054068 (2018).
42. Zeng, L. et al. Measuring phonon mean free path distributions by probing quasiballistic phonon transport in grating nanostructures. *Sci. Rep.* **5**, 17131 (2015).
43. Frazer, T. D. et al. Engineering nanoscale thermal transport: size- and spacing-dependent cooling of nanostructures. *Phys. Rev. Appl.* **11**, 024042 (2019).
44. Landry, E. S. & McGaughey, A. J. Effect of film thickness on the thermal resistance of confined semiconductor thin films. *J. Appl. Phys.* **107**, 013521 (2010).
45. Ziabari, A. et al. Full-field thermal imaging of quasiballistic crosstalk reduction in nanoscale devices. *Nat. Commun.* **9**, 255 (2018).
46. Ziman, J. M. *Electrons and Phonons* (Clarendon Press, Oxford, 1960).
47. McGaughey, A. J. H., Jain, A., Kim, H.-Y. & Fu, B. Phonon properties and thermal conductivity from first principles, lattice dynamics, and the Boltzmann transport equation. *J. Appl. Phys.* **125**, 011101 (2019).
48. Feng, T., Lindsay, L. & Ruan, X. Four-phonon scattering significantly reduces intrinsic thermal conductivity of solids. *Phys. Rev. B* **96**, 161201 (2017).
49. Lee, S.-M. & Cahill, D. G. Heat transport in thin dielectric films. *J. Appl. Phys.* **81**, 2590–2595 (1997).
50. Li, D., Wu, Y., Fan, R., Yang, P. & Majumdar, A. Thermal conductivity of Si/SiGe superlattice nanowires. *Appl. Phys. Lett.* **83**, 3186–3188 (2003).
51. Giri, A., Braun, J. L., Rost, C. M. & Hopkins, P. E. On the minimum limit to thermal conductivity of multi-atom component crystalline solid solutions based on impurity mass scattering. *Scr. Materialia* **138**, 134–138 (2017).
52. Giri, A., Braun, J. L. & Hopkins, P. E. Reduced dependence of thermal conductivity on temperature and pressure of multi-atom component crystalline solid solutions. *J. Appl. Phys.* **123**, 015106 (2018).

53. Liang, Z., Sasikumar, K. & Keblinski, P. Thermal transport across a substrate–thin-film interface: effects of film thickness and surface roughness. *Phys. Rev. Lett.* **113**, 065901 (2014).
54. Liang, Z. & Keblinski, P. Finite-size effects on molecular dynamics interfacial thermal-resistance predictions. *Phys. Rev. B* **90**, 075411 (2014).
55. Lee, E., Zhang, T., Hu, M. & Luo, T. Thermal boundary conductance enhancement using experimentally achievable nanostructured interfaces - analytical study combined with molecular dynamics simulation. *Phys. Chem. Chem. Phys.* **18**, 16794–16801 (2016).
56. Giri, A. et al. Interfacial defect vibrations enhance thermal transport in amorphous multilayers with ultrahigh thermal boundary conductance. *Adv. Mater.* **30**, 1804097 (2018).
57. Lee, E., Zhang, T., Yoo, T., Guo, Z. & Luo, T. Nanostructures significantly enhance thermal transport across solid interfaces. *ACS Appl. Mater. Interfaces* **8**, 35505–35512 (2016).
58. Chen, G. Size and interface effects on thermal conductivity of superlattices and periodic thin-film structures. *J. Heat. Transf.* **119**, 220–229 (1997).
59. Liang, Z., Sasikumar, K. & Keblinski, P. Thermal transport across a substrate-thin film interface: effect of film thickness and surface roughness. *Phys. Rev. Lett.* **113**, 065901 (2014).
60. Giri, A. & Hopkins, P. E. A review of experimental and computational advances in thermal boundary conductance and nanoscale thermal transport across solid interfaces. *Adv. Funct. Mater.* **30**, 1903857 (2020).
61. Zaccone, A. & Baggioli, M. Universal law for the vibrational density of states of liquids. *Proc. Natl Acad. Sci.* **118**, e2022303118 (2021).
62. Plimpton, S. Fast parallel algorithms for short-range molecular dynamics. *J. Comput. Phys.* **117**, 1–19 (1995).
63. Stillinger, F. H. & Weber, T. A. Computer simulation of local order in condensed phases of silicon. *Phys. Rev. B* **31**, 5262–5271 (1985).
64. Schelling, P. K., Phillpot, S. R. & Keblinski, P. Comparison of atomic-level simulation methods for computing thermal conductivity. *Phys. Rev. B* **65**, 144306 (2002).
65. Larkin, J. M. & McGaughey, A. J. H. Thermal conductivity accumulation in amorphous silica and amorphous silicon. *Phys. Rev. B* **89**, 144303 (2014).
66. Abs da Cruz, C., Termentzidis, K., Chantrenne, P. & Kleber, X. Molecular dynamics simulations for the prediction of thermal conductivity of bulk silicon and silicon nanowires: Influence of interatomic potentials and boundary conditions. *J. Appl. Phys.* **110**, 034309 (2011).
67. Jiang, J.-W., Park, H. S. & Rabczuk, T. Molecular dynamics simulations of single-layer molybdenum disulphide (MoS2): Stillinger-Weber parametrization, mechanical properties, and thermal conductivity. *J. Appl. Phys.* **114**, 064307 (2013).
68. Thakur, S. & Giri, A. Role of anharmonicity in dictating the thermal boundary conductance across interfaces comprised of two-dimensional materials. *Phys. Rev. Appl.* **20**, 014039 (2023).
69. Sellan, D. P., Landry, E. S., Turney, J. E., McGaughey, A. J. H. & Amon, C. H. Size effects in molecular dynamics thermal conductivity predictions. *Phys. Rev. B* **81**, 214305 (2010).
70. Chen, L., Wang, X. & Kumar, S. Thermal transport in fullerene derivatives using molecular dynamics simulations. *Sci. Rep.* **5**, 12763 (2015).
71. Chen, Y., Li, D., Lukes, J. R., Ni, Z. & Chen, M. Minimum superlattice thermal conductivity from molecular dynamics. *Phys. Rev. B* **72**, 174302 (2005).
72. Giri, A., Donovan, B. F. & Hopkins, P. E. Localization of vibrational modes leads to reduced thermal conductivity of amorphous heterostructures. *Phys. Rev. Mater.* **2**, 056002 (2018).
73. Dionne, C. J. & Giri, A. Magnesium doping enhances thermal conductivity of polymerized fullerene crystals. *J. Phys. Chem. C.* **126**, 17406–17414 (2022).

Acknowledgements

A.G. is supported by the Office of Naval Research, Grant No. N00014-24-1-2419. P.E.H is supported by the Army Research Office, Grant No. W911NF-21-1-0119 and the National Science Foundation (NSF Award No. 2318576).

Author contributions

C.J.D. performed the thermal conductivity, temperature profile, density of states, heat flux, and wave packet calculations. S.T. performed the spectral energy density calculations. N.S. performed the diffusive temperature profile calculations. C.J.D. and A.G. interpreted the results with contributions from S.T. and P.E.H. C.J.D., A.G. and P.E.H wrote the original draft and all authors edited, revised and approved the paper. A.G. conceived the project and acquired the funding.

Competing interests

The authors declare no competing interests.

Additional information

Supplementary information The online version contains supplementary material available at https://doi.org/10.1038/s41524-024-01364-w.

Correspondence and requests for materials should be addressed to Ashutosh Giri.